WPPFC-CPR(18) 18818

R Mateus et al.

Analysis of retained deuterium on Be-O films: ion implantation vs. in-situ loading

Preprint of Paper to be submitted for publication in Proceeding of 23rd International Conference on Plasma Surface Interactions in Controlled Fusion Devices (PSI-23)

This work has been carried out within the framework of the EUROfusion Consortium and has received funding from the Euratom research and training programme 2014-2018 under grant agreement No 633053. The views and opinions expressed herein do not necessarily reflect those of the European Commission.

Analysis of retained deuterium on Be-based films: ion implantation vs. in-situ loading

R. Mateus[a,*], C. Porosnicu[b], C.P. Lungu[b], C. Cruz[a], Z. Siketić[c], I. Bogdanovic Radovic[c], A. Hakola[d], E. Alves[a] and WP PFC contributors[e]

[a]*Instituto de Plasmas e Fusão Nuclear, Instituto Superior Técnico, Universidade de Lisboa, 1049-001 Lisboa, Portugal*

[b]*National Institute for Lasers, Plasma and Radiation Physics, Bucharest 077125, Romania*

[3]*Ruder Bošković Institute, P.O. Box 180, 10002 Zagreb, Croatia*

[c]*VTT Technical Research Centre of Finland Ltd, P. O. Box 1000, 02044 VTT, Finland*

[e]*see the author list in "S. Brezinsek et al., 2017 Nucl. Fusion 57 116041"*

*corresponding author: rmateus@ipfn.ist.utl.pt

Abstract

Pure Be, Be-O and Be-O-C thin coatings were deposited by using the high-power impulse magnetron sputtering (HiPIMS) method with and without incorporation of deuterium. The coatings produced without deuterium were implanted afterwards by energetic 15 keV $^2H^+$ ion beams with a fluence limited to 2 x 10^{17} ion/cm^2 in order to mitigate the damage imposed by ion irradiation and prevent a fast gas release. The as-deposited and as-implanted coatings were analysed by IBA techniques, namely by elastic and Rutherford backscattering (EBS and RBS, respectively), nuclear reaction analysis (NRA) and by time-of-flight elastic recoil detection analysis (ToF-ERDA). Despite distinct deuterium depth profiles in the implanted samples, the results show that for the present ion implantation and deposition parameters, similar retained amounts are revealed in the films loaded by ion implantation or during the HiPIMS deposition, assuring ion implantation as a competitive method for fuel incorporation in thin Be-based films.

Keywords: beryllium coatings, deuterium, HiPIMS, ion implantation

1. Introduction

ITER-relevant coatings containing beryllium (Be) are being developed within the EUROfusion Work Programme to produce standard samples for fuel retention investigations. Previous experiments involved the Thermionic Vacuum Arc (TVA) method to deposit Be-based films containing tungsten (W), oxygen (O) and carbon (C) followed by irradiation campaigns with deuterium (identified in the text as D or as the $^2H^+$ ion)

ion beams [1]. Co-deposition of D by TVA was also performed with satisfactory results. Presently, deuterium is being incorporated in mixed samples to mimic the trapping of nuclear fuel in PFC co-deposits by two loading methods: in-situ during the deposition of the coatings by using a more efficient plasma vapor deposition technique for D incorporation [2], the high-power impulse magnetron sputtering (HiPIMS) method [2-4], or by ion implantation of $^{2}H^{+}$ ions on equivalent non-doped samples [5]. Recently, Be co-deposits containing C were found in the divertor tiles of the JET-ILW experiment, being the origin of the C source related with the use of W-coated carbon fibre composites (CFC) [6]. Therefore, and additionally to the role of O on fuel retention mechanisms, the presence of C has aroused a new interest in the study of the Be-O-C-D system. W-coated CFC components will be not installed in ITER and therefore, fuel retention studies involving the JET-ILW environment should be interpreted as an upper limit of the retention mechanisms in ITER [7].

New data show that the D content in mixed HiPIMS Be layers may be enhanced up to 30-40 at.% by C incorporation and by increasing the thickness of the coatings to several microns [2]. Nevertheless, the retained fuel deeply decreases when the same methods are used to load thinner samples. In this sense, a comparative study involving controlled plasma deposition methods and ion implantation is being implemented in order to establish the ion implantation technique as a competitive method for the production of some of the thin Be standards. Here we report the first experimental results from thin Be, Be-O and Be-C-O films grown with and without D seeding by HiPIMS. The samples without a D content were implanted afterwards by energetic $^{2}H^{+}$ ions. The resulting layers were investigated by ion beam analysis (IBA). All the samples were produced with a nominal thickness of 400 nm. W was the primary choice for the substrate material, while this is the composition of the divertor of the JET-ILW. The use of Si substrates is attractive considering the production of a huge amount of samples and therefore, thin Be-based films were deposited in both W and Si plates. The efficiency of the two methods for D incorporation, ion implantation and in-situ loading, and a possible role imposed by the W and Si pure substrates in the gas release could be also compared.

2. Experiment and methods

2.1 Deposition of Be-based films

Before deposition, the W and Si plates were polished up to a mirror-like quality and mounted on the sample holder located at the centre of the reaction chamber. The partial pressures of Ar, used as background gas, and of O_2 and D_2 prior atmospheres (the O and D gas source) were calibrated with mass flow controllers installed in inlet ports for the gaseous elements. As sources for Be and C, pure circular rods were used as solid targets during the sputtering process of HiPIMS [2-4], a plasma vapour deposition technique providing high pulse power densities at very low duty cycles and high plasma and ionization densities with energetic sputtered ions [4]. The deposition rate was monitored using a quartz crystal microbalance located close to

the substrates. The deposition time was selected to produce thin coatings with the desired thicknesses of 400 nm.

The 400 nm samples were the first ones of a wide group of Be-based coatings deposited with thicknesses as high as 15 μm [2], and therefore the initial procedures were used to calibrate the final thicknesses and stoichiometries for the entire set. The main goals achieved during the present depositions were a better control of the deposition rates for Be and C, which directly depend on the HiPIMS discharges, the control of the accumulation of O, enhanced by the affinity of Be to react with O, particularly in the case of thin depositions, and the production of uniform depth profiles. Table 1 exhibits the goal compositions of the 400 nm coatings selected for the experiment, based on stoichiometries already observed in JET-ILW deposits. Some of the Be coatings revealed compositions too distinct from those of Table 1. Nevertheless, they are appropriate to compare the retention of fuel in thin samples achieved by ion implantation or by in-situ loading.

2.2 Implantation of deuterium ions

Enhanced structural modifications in Be-based materials occur under energetic ion bombardment. Earlier irradiation experiments of Be plates performed with energetic $^2H^+$ ions (~10 keV) at room temperature (RT) indicated 2 x 10^{17} ion/cm^2 as the fluence limit above which diluted D becomes saturated on a Be lattice and nano-cavities filled by molecular D_2, (starting at about 3 x 10^{16} ion/cm^2) start to form nano-channels enabling fast release of D [6]. Therefore, for the present experiment the fluences of D irradiations at RT were restricted to the above-mentioned 2 x 10^{17} ion/cm^2 with the purpose to preserve the structural integrity of the coatings [8]. Current densities lower than 1.0 μA/cm^2 and power densities as high as 0.03 W/cm^2 assured no heating event to occur during irradiations.

Beryllium oxide (BeO) has a mass density close to 3.02 g/cm^3 (the equivalent atomic density is 12.34 x 10^{22} atoms/cm^3) and a BeO component is always present inside Be matrixes that typically have a mass density of 1.85 g/cm^3 (14.49 x 10^{22} atoms/cm^3). The addition of C should not change at much the final densities and therefore, during the preparatory work of the irradiation campaign, simulations of the depth profiles of D in BeO and in pure Be were carried out using the SRIM software [9] considering different incident energy beams. The use of 15 keV $^2H^+$ ion beams assures that most of the retained D remains deeply inside the Be-based coatings with nominal thicknesses of 400 nm, and the incident energy of 15 keV was chosen for the entire irradiation campaign. Depth profiles for the induced irradiation damages and for the retained D contents of the coating were quantified considering fluences of 2 x 10^{17} ion/cm^2 and 15 keV $^2H^+$ incident ions on BeO and on pure Be. In these experiments we did not consider sputtering or erosion of the irradiated surfaces and therefore, the damage profiles were quantified with the mode “Detailed calculations with full damage cascades” by using default values for the displacement energies of Be and of O atoms, 25 eV and 28 eV,

respectively, and for the lattice binding energies, which are 3 eV for both elements [9,10]. The main contributions for the final damages are caused by vacancies on both Be and O locations in the BeO lattice, and by the vacancies on Be locations in pure Be. Obviously, the evaluations with the SRIM code do not take into account the existence of lattice defects, of trapping sites on the grain boundaries, or even of structural inclusion in the films.

2.3 Ion beam analysis

The elemental depth composition of the as-grown HIPIMS and of the as-implanted coatings were analysed by elastic backscattering spectrometry (EBS) carried out with incident 1500 keV or 1600 keV $^{1}H^{+}$ ion beams in order to maximize simultaneously the sensitivity for the detection of Be [11], C and O [12] enhancing the non-Rutherford scattering of protons by ^{9}Be [11], and by ^{12}C and ^{16}O [12]. The non-Rutherford cross-sections for C and O were calculated using the SigmaCalc software [12]. The analysis of the EBS spectra took into account the yields arising from the emission of deuterium and alpha particles induced by the $^{9}Be(p,d)^{8}Be$ and $^{9}Be(p,\alpha)^{6}Li$ nuclear reactions [11]. For a better sensitivity in thickness evaluations, Rutherford backscattering (RBS) analysis was carried out with incident 2000 keV $^{4}He^{+}$ ion beams. Both EBS and RBS spectra were collected at a scattering angle of 165° [11,12]. Finally, the quantification for D was carried out by nuclear reaction analysis (NRA) involving incident 1000 keV or 2200 keV $^{3}He^{+}$ ion beams and the proton yields emitted from the $^{2}H(^{3}He,p)^{4}He$ reaction [13] at a scattering angle of 140°. The cross-sections of the nuclear reaction are about 3.5 higher at 1000 keV than at 2200 keV and the lower energy is the obvious choice for the analysis of low D contents in thin samples. The higher energy was just used during the analysis of additional Be-based thick samples [2], outside the scope of the present experiment, in order to enhance the depth resolution for D quantification. In this case, the D contents quantified from the $^{2}H(^{3}He,p)^{4}He$ proton yields were normalized with the corresponding yields induced by the $^{9}Be(^{3}He,p_{0})^{11}B$ emission [14], also present in the NRA spectra. The elemental quantifications were performed with the NDF code [15], enabling a simultaneous analysis of distinct spectra collected from different techniques such as EBS, RBS and NRA. The cross-section for the Rutherford scattering linearly depends on the square of the atomic number of the target nuclei. Therefore and due to the superposition of the elemental scattering yields, the sensitivity to quantify the surface densities of light elements in thin films from the measured EBS spectra is challenging when heavy substrate materials are used. For this reason, the C and O contents of the samples were preferentially quantified with EBS spectra collected from coatings deposited on Si substrates. Results of the analytical procedure are shown in Fig. 2 for the case of Be+O (90:10) coatings deposited on Si.

Three months after implantation, the implanted samples were additionally analysed by time-of-flight elastic recoil detection (ToF-ERDA). The spectrometer was positioned at an angle of 37.5° with respect to the beam direction, and 23 MeV $^{127}I^{6+}$ ion beams at an incident angle of 20° were used to evaluate the elemental

depth profile of a large number of elements along the superficial layers and the release behaviour of D from the implanted surfaces [16]. The quantifications were performed with the Potku code [17], which allows evaluating possible changes in the superficial composition during the collection of the spectra. Examples of the changes may include the release of non-bound D during the analysis.

3. Results and discussion

Fig. 1(a) presents the simulated depth profiles for the atomic content of retained D in a mixed Be+O (1:1) layer, representing a beryllium oxide (BeO) lattice and stoichiometry, and in pure Be after implantation, pointing to medium depth ranges (Rp) with straggling (ΔRp) of 193 nm and 44 nm for BeO and of 256 nm and 46 nm for pure Be, respectively. The smaller depth ranges of implanted D for BeO relatively to pure Be evidence the different atomic densities of BeO (14.49×10^{22} atoms/cm^3) and of Be (12.34×10^{22} atoms/cm^3) and also the (electronic and nuclear) energy losses imposed by the two materials to the impinging ions. The irradiation with a fluence of 2×10^{17} ion/cm^2 energetic 15 keV $^2H^+$ ions resulted in maximum D contents close to 1.40 at.% for BeO and 1.55 at.% for Be predicted for the medium depth ranges (Rp). The corresponding depth profiles of the damage cascades along the path of the impinging ions are presented in Fig. 1(b). The same fluence of 2×10^{17} ion/cm^2 was considered for the calculations. As observed in the figure, the predicted irradiation damage peaks are at lower depths with respect to Rp and are found at 180 nm in BeO and 240 nm in Be. The corresponding maximum irradiation damages are moderate and close to 0.21 dpa and 0.17 dpa, pointing to low structural modification imposed by the present irradiations. The evaluation of the total damage depth profile induced in BeO considered the individual elemental contributions of Be and of O (the density of created vacancies in Be (green line) and in O locations (blue line), mainly), as visualised in Fig. 1(b). The sum of both Be and O contribution is also shown (dashed line).

As an example of the analytical procedure carried out during the simultaneous EBS, RBS and NRA chemical analyses [15], Fig. 2(a) presents the EBS spectrum and corresponding fit line achieved from the use of an incident 1600 keV $^1H^+$ ion beam in one of the Be+O (90:10) coatings deposited on a Si substrate. The identification of the Be, O and Si peaks are associated with elastic scattering of protons by (the major contributions of the isotopes) ^{9}Be, ^{16}O and ^{28}Si. The yield of the $^9Be(p,d_0)^8Be$ nuclear reaction is also identified in the spectrum while the yield of the $^9Be(p,\alpha_0)^6Li$ reaction is hindered due to the presence of a high O content. In Fig. 2(b) and 2(c) the arrows denote the energies corresponding to the presence of Be, O, Si and D (^{2}H) on the surface layer. A better sensitivity for thickness evaluation in the same coating is achieved by RBS with a 2000 keV $^4He^+$ ion beam. This is visualized by the shift of the Si yield (the substrate) towards lower energies in Fig. 2(b) (the vertical arrow for Si mark the corresponding position for Si if it is on the surface). The thickness of the O signal in the spectrum also evidences a high O content along the entire coating's depth. Finally, the corresponding D content is quantified by NRA (Fig. 2(c)) by

resolving the yield of the $^{2}H(^{3}He,p_0)^{4}He$ proton emission. In the present case, where 1000 keV $^{3}He^{+}$ beams were used, low yields arising from the $^{9}Be(^{3}He,p_i)^{11}B$ proton emissions can be seen [14].

A similar method was applied for the analysis of all samples. The results of the EBS, RBS and NRA analyses are summarised by presenting the quantified D content (in 10^{17} at/cm^2 units), the thickness (in 10^{17} at/cm^2 units) and the atomic elemental composition (at.%) for D, Be, O and C in each individual coating. Sometimes, more than one layer was needed to characterize the composition through the entire films depth. Table 2 and Table 3 present the results achieved from the as-implanted and from the coatings already containing D, respectively. After implantation the relative Be, C and O stoichiometries remain the same, and therefore, the results for the coatings before implantation are not presented.

Three main features may be identified from the analysis. The first one shows that was difficult to control the O concentration in the deposition due to the affinity of superficial Be to react with O and typically, high O amounts were preferentially co-deposited in the thin Be+O and Be+O+C coatings. The same behaviour is observed in Be co-deposits in operative plasma scenarios. The second feature is that the mean atomic fraction for the retained D in the as-implanted coatings is higher than the values predicted from SRIM evaluations, where maximum D contents are close to 1.5 at.% (see Fig. 1). This is observed from the data of the implanted Be and Be+O coatings, and the feature need to be related with the corresponding microstructures, while similar atomic D concentration are also achieved from the coatings grown in-situ with D (Table 2 and Table 3). Obviously, the presence of C in Be+O+C films tends to enhance the retention of D (Table 2 and Table 3). The result is in line with the main conclusion of the analysis of the entire set of thin and thick HiPIMS Be-based coatings [2]. A last evidence of the present experiment reveals that in the case of Be+O+C coatings most of the implanted ions became retained on the substrate. This is revealed by the measured film thickness and by the huge atomic contents quantified for D in these particular samples (Table 2). The depth resolution of the present NRA technique is not high enough to distinguish depth ranges in the nm depth scale and therefore, higher atomic contents were considered to resolve the corresponding $^{2}H(^{3}He,p_0)^{4}He$ proton yields. The elemental depth profiles quantified by ToF-ERDA confirmed the assumption.

Finally, ToF-ERDA analyses confirmed the main results obtained by EBS, RBS and NRA. The technique is very sensitive to the composition of the superficial layers and therefore, Table 4 mainly resumes the D, Be, O and C composition achieved for a depth range of 1 x 10^{18} at/cm^2. The ToF-ERDA 2D coincidence maps enable a clear separation of the signals arising from different elements or isotopes providing at.% as well as depth profiles for all species in the films. Fig. 3(a) shows the coincident map collected from the same sample presented in Fig. 2, the implanted Be+O (90:10) coating deposited on Si. The corresponding depth profiles achieved for the major and for the minor elements are shown in Fig. 3(b) and 3(c), respectively. The analysis confirms the main BeO composition of the film and the presence of implanted D along the deeper zone of the coating. A minor amount of C is also present throughout the coating as a contaminant, ^{1}H is an obvious

environmental contamination and residual amounts of Ar, the background gas of the HiPIMS deposition, are also visible on the surface. At the deeper depth zones, the profile of D follows the depth profile for C and therefore, we may conclude that D is only present within the Be+O material and not in the Si substrate. By comparing the results of the NRA analyses with the ToF-ERDA ones performed three months after, we confirm a typical degassing behaviour in the coatings. Nevertheless, three months after implantation the retained D seems to be about 30% lower, pointing to life-times of several months for the implanted coatings, which are suitable enough for dedicated retention experiments in the future. It is not possible to confirm different retention behaviours from the use of Si or W plates as substrate, meaning that the substrate material is not playing an important role in D retention.

By comparing the retention results of the as-implanted coatings (Table 2) and of the ones with already deposited D (Table 3), we conclude that the ion implantation technique is competitive enough to deposit D in thin films. The implantation of energetic $^{2}H^{+}$ ions in Be-based materials at moderated fluences may reduce the damage imposed to the coating's structure, increasing the life-time of the produced samples.

Recently, multiple irradiation stages were performed in W-O coatings to load both He [18] or D species by ion implantation in order to enhance the final retention ratios. Higher incident beam energy was applied during the first stage, and the energy was successively reduced in the subsequent stages. The depth profiles visualized in Fig. 1 point to the future use of the same method to load higher amounts of D in Be-based coatings, leading to the broadening of the corresponding depth profiles of implanted D and of the induced irradiation damage, retarding the saturation of the matrix by D incorporation. Total fluences as high as 2 x 10^{17} ion/cm^{2} could be used, once again, in order to mitigate the irradiation damage effects and degassing mechanism.

4. Conclusions

Be, Be+O and Be+O+C thin coatings were produced by HiPIMS and were implanted afterwards at RT by energetic 15 keV $^{2}H^{+}$ ions with a moderate fluence of 2 x 10^{17} ion/cm^{2} in order to mitigate the irradiation damage effects. In parallel, coatings of similar thickness and composition but with D inclusions were also deposited by HiPIMS. The retained D amounts quantified with IBA techniques, in particular by using EBS, RBS, NRA and ToF-ERDA, proves that for the particular use of thin coatings, ion implantation is a competitive technique to load deuterium in the present Be-based coating. The life-time of the enriched samples is high enough to extend the experiments in months. Future D loading on the same coatings may include multiple implantation stages and similar ion fluences to broad the depth profiles for D contents and for the induced irradiation damage, retarding the saturation of the Be-based matrix by D and the degassing of the implanted material.

Acknowledgements

This work has been carried out within the framework of the EUROfusion Consortium and has received funding from the Euratom research and training programme 2014-2018 under grant agreement number 633053. The views and opinions expressed herein do not necessarily reflect those of the European Commission. Work performed under EUROfusion WP PFC. IST also received financial support from "Fundação para a Ciência e a Tecnologia" through project UID/FIS/50010/2013.

References

[1] K. Sugiyama, C. Porosnicu, W. Jacob, I. Jepu, C. P. Lungu, Investigation of deuterium retention in/desorption from beryllium-containing mixed layers, Nucl. Mater. Energy 6 (2016) 1-9.

[2] A. Hakola et al., Production of ITER-relevant Be-containing laboratory samples for fuel retention investigations, these proceedings.

[3] P. Dica et al., Beryllium-tungsten study on mixed layers obtained by m-HiPIMS/DCMS techniques in a deuterium and nitrogen reactive gas mixture, Surf. Coat. Technol. 321 (2017) 397-402.

[4] I.-L. Velicu et al., Enhanced properties of tungsten thin films deposited with a novel HiPIMS approach, Appl. Surf. Sci. 424 (2017) 397.

[5] R. Mateus, A. Hakola, V. Tiron, C. Porosnicu, C.P. Lungu, E. Alves, Study of deuterium retention in Be-W coatings with distinct roughness profiles, Fusion Eng. Des. 124 (2017) 464.

[6] M. Maier et al., Erosion and deposition in the JET divertor during the first ILW campaign, Phys. Scr. T167 (2016) 014051.

[7] N. Catarino et al., Assessment of erosion, deposition and fuel retention in the JET-ILW divertor from ion beam analysis data, Nucl. Mater. Energy 12 (2017) 559-563.

[8] V.N. Chemikov et al., Gas-induced swelling of beryllium implanted with deuterium ions, J. Nucl. Mater. 233-237 (1996) 860-864.

[9] J.F. Ziegler, M.D. Ziegler, J.P. Biersack, SRIM - The stopping and range of ions in matter (2010), Nucl. Inst. Methods Phys. Res. B 268 (2010) 1818.

[10] J Byggmästar, E A Hodille , Y Ferro, K Nordlund, Analytical bond order potential for simulations of BeO 1D and 2D nanostructures and plasma-surface interactions, J. Phys. Condens. Matter 30 (2018) 135001.

[11] N. Catarino, N.P. Barradas, E. Alves, Determination of $^{9}Be(p,p_0)^{9}Be$, $^{9}Be(p,d_0)^{8}Be$ and $^{9}Be(p,\alpha_0)^{6}Li$ cross sections at 150° in the energy range 0.5–2.35MeV**,** Nucl. Inst. Methods Phys. Res. B 371 (2016) 50.

[12] A.F. Gurbich, SigmaCalc recent development and present status of the evaluated cross-sections for IBA**,** Nucl. Inst. Methods Phys. Res. B 371 (2016) 27.

[13] W. Moller, F. Besenbacher, A note on the ^{3}He + D nuclear-reaction cross section, Nucl.Instr.Meth. 168 (1980) 111-114.

[14] N.P. Barradas et al, Determination of the $^{9}Be(^{3}He,pi)^{11}B$ (i = 0,1,2,3) cross section at 135° in the energy range 1-2.5 MeV, Nucl. Inst. Methods Phys. Res. B 346 (2015) 21.

[15] N.P. Barradas, C. Jeynes, R.P. Webb, Simulated annealing analysis of Rutherford backscattering data, Appl. Phys. Lett. 71 (1997) 291–293.

[16] Z. Siketić, N. Skukan, I. Bogdanović Radović, A gas ionisation detector in the axial (Bragg) geometry used for the Time-of-Flight Elastic Recoil Detection Analysis, Rev. Sci. Instrum. 86 (2015) 083301.

[17] K. Arstila, et al., Potku – New analysis software for heavy ion elastic recoil detection analysis, Nucl. Inst. Methods Phys. Res. B 331 (2014) 34-41.

[18] R. Mateus et al., Helium load on W-O coatings grown by pulsed laser deposition, Surface & Coatings Technology (2018), https://doi.org/10.1016/j.surfcoat.2018.02.089

Table 1
Nominal compositions of Be coatings deposited by HiPIMS.

Nominal composition	Nominal stoichiometry	Nominal composition	Nominal stoichiometry
Be on Si	-	Be+D on Si	(100:5)
Be+O on Si	(95:5)	Be+O+D on Si	(95:5:5)
Be+O on Si	(90:10)	Be+O+D on Si	(90:10:5)
Be+O+C on Si	(90:5:5)	Be+O+C+D on Si	(90:5:5:5)
Be+O+C on Si	(84:8:8)	Be+O+C+D on Si	(84:8:8:5)
Be on W	-	Be+D on W	(100:5)
Be+O on W	(95:5)	Be+O+D on W	(95:5:5)
Be+O on W	(90:10)	Be+O+D on W	(90:10:5)
Be+O+C on W	(90:5:5)	Be+O+C+D on W	(90:5:5:5)
Be+O+C on W	(84:8:8)	Be+O+C+D on W	(84:8:8:5)

Table 2.
Elemental depth composition of as-implanted coatings as quantified by EBS, RBS and NRA.

Nominal composition	Nominal stoichiometry	Total D content (10^{17} at/cm^2)	Layer	Thickness (10^{17} at/cm^2)	D (at.%)	Be (at.%)	O (at.%)	C (at.%)
Be on Si	-	0.82	1	24.0	2.63	89.6	7.8	-
			2	11.0	2.63	63.3	34.1	-
Be+O on Si	(95:5)	0.96	1	51.0	1.89	49.1	49.1	-
Be+O on Si	(90:10)	0.62	1	40.5	1.53	49.2	49.2	-
Be+O+C on Si	(90:5:5)	1.87	1	5.5	8.42	62.3	18.3	11.0
			2	3.5	7.85	58.0	23.9	10.2
			3	11.5	9.87	73.0	4.3	12.9
			4	6.0	0.00	63.0	25.9	11.1
Be+O+C on Si	(84:8:8)	1.91	1	25.0	7.63	39.0	46.6	6.8
Be on W		1.16						
Be+O on W	(95:5)	1.23						
Be+O on W	(90:10)	0.89						
Be+O+C on W	(90:5:5)	1.80						
Be+O+C on W	(84:8:8)	0.63						

Table 3.
Elemental depth composition of as-deposited coatings grown with D as quantified by EBS, RBS and NRA.

Nominal composition	Nominal stoichiometry	Total D content (10^{17} at/cm^2)	Layer	Thickness (10^{17} at/cm^2)	D (at.%)	Be (at.%)	O (at.%)	C (at.%)
Be+D on Si	(100:5)	1.89	1	57.5	3.29	95.7	1.0	-
Be+O+D on Si	(95:5:5)	0.48	1	46.0	1.04	49.5	49.5	-
Be+O+D on Si	(90:10:5)	0.62	1	35.0	1.77	49.1	49.1	-
Be+O+C+D on Si	(90:5:5:5)	1.02	1	5.0	3.70	79.4	9.9	6.9
			2	3.5	3.70	44.0	45.1	7.2
			3	13.0	3.70	87.1	2.0	7.2
			4	6.0	3.70	66.6	22.5	7.2
Be+O+C+D on Si	(84:8:8:5)	0.80	1	14.5	2.36	40.6	53.8	3.3
			2	1.3	2.50	87.0	7.0	3.5
			3	10.0	2.36	47.2	47.2	3.3
Be+D on W	(100:5)	2.21						
Be+O+D on W	(95:5:5)	0.76						
Be+O+D on W	(90:10:5)	0.52						
Be+O+C+D on W	(90:5:5:5)	1.10						
Be+O+C+D on W	(84:8:8:5)	1.21						

Table 4.
Elemental depth composition of aged implanted coatings as quantified by TOF-ERDA.

Nominal composition	Nominal stoichiometry	Thickness (10^{17} at/cm^2)	Total D content (10^{17} at/cm^2)	Be (at.%)	O (at.%)	C (at.%)
Be on Si	-	32.4	1.10	88.5	6.3	-
Be+O on Si	(95:5)	53.7	0.67	45.2	48.2	1.4
Be+O on Si	(90:10)	37.5	0.20	49.2	49.2	-
Be+O+C on Si	(90:5:5)	25.0	1.70	48.0	17.0	11.5
Be+O+C on Si	(84:8:8)	17.5	1.90	40.0	48.0	2.7
Be on W		33.3	1.00	85.0	7.4	-
Be+O on W	(95:5)	-	0.92	39.0	44.0	2.4
Be+O on W	(90:10)	39.0	0.78	44	50	-
Be+O+C on W	(90:5:5)	25.0	1.90	58.0	16.0	11.1
Be+O+C on W	(84:8:8)	22.0	0.55	39.0	44.0	2.2

Figure Captions

Fig. 1. Simulated depth profiles of D on Be and on BeO, i.e. Be+O having the (1:1) stoichiometry (a); corresponding irradiation damage induced by irradiating a fluence of 2 x 10^{17} ion/cm^2 15 keV $^2H^+$ ions (b). The individual contributions of the induced Be vacancies (green line) and O vacancies (blue line) in the total damage of the Be+O lattice (dashed line) are also represented in (b).

Fig. 2. EBS, (a), RBS (b) and NRA (c) spectra and corresponding fit lines achieved from the chemical analysis performed on Be+O (90:10) coating deposited on Si. EBS and the RBS experiments were carried out with 1600 keV $^1H^+$ and 2000 keV $^4He^+$ incident ion beams, respectively, at a scattering angle of 165°. The NRA spectrum was collected using incident 1000 keV $^3He^+$ ion beams at a scattering angle of 140°.

Fig. 3. ToF-ERDA 2D coincidence maps of a Be+O (90:10) coating deposited on Si after D implantation (a) with quantified elemental depth profiles for Be and O (b) and for ^1H, ^2H, C and Ar (c).

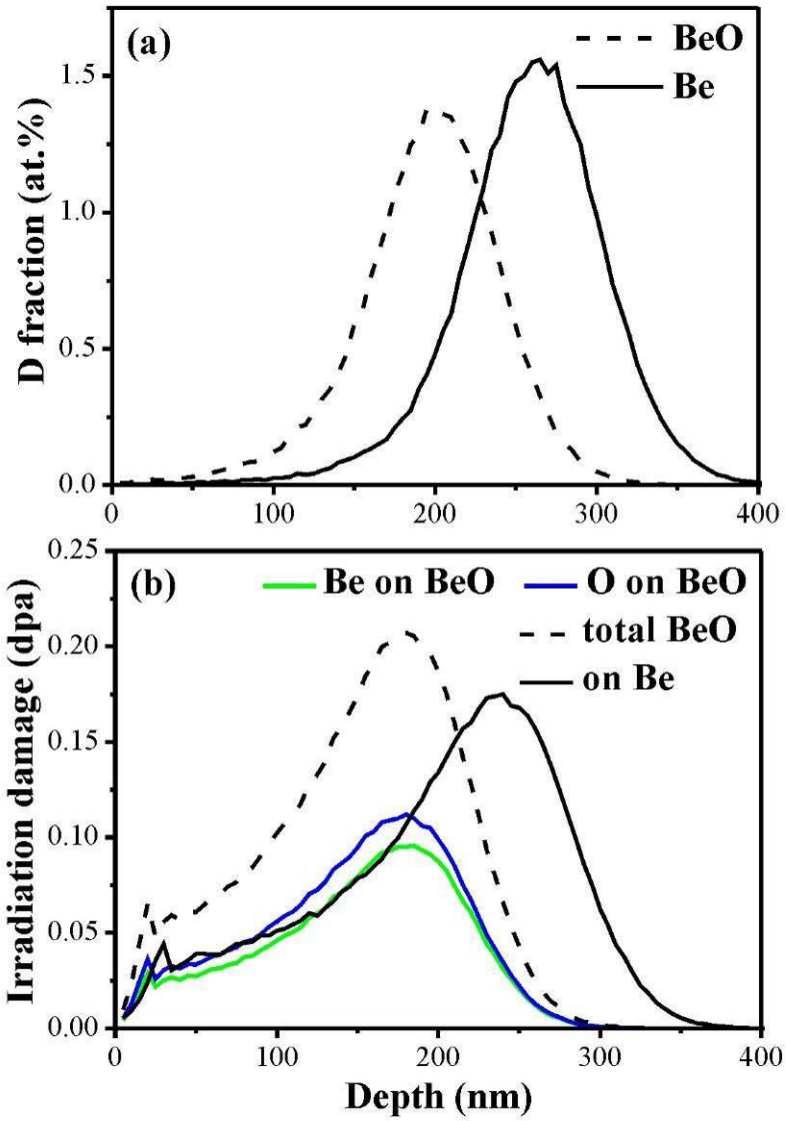
(a)
BeO
Be
D fraction (at.%)
1.5
1.0
0.5
0.0
0
100
200
300
400
(b)
Be on BeO
O on BeO
total BeO
on Be
Irradiation damage (dpa)
0.25
0.20
0.15
0.10
0.05
0.00
0
100
200
300
400
Depth (nm)

Fig. 1

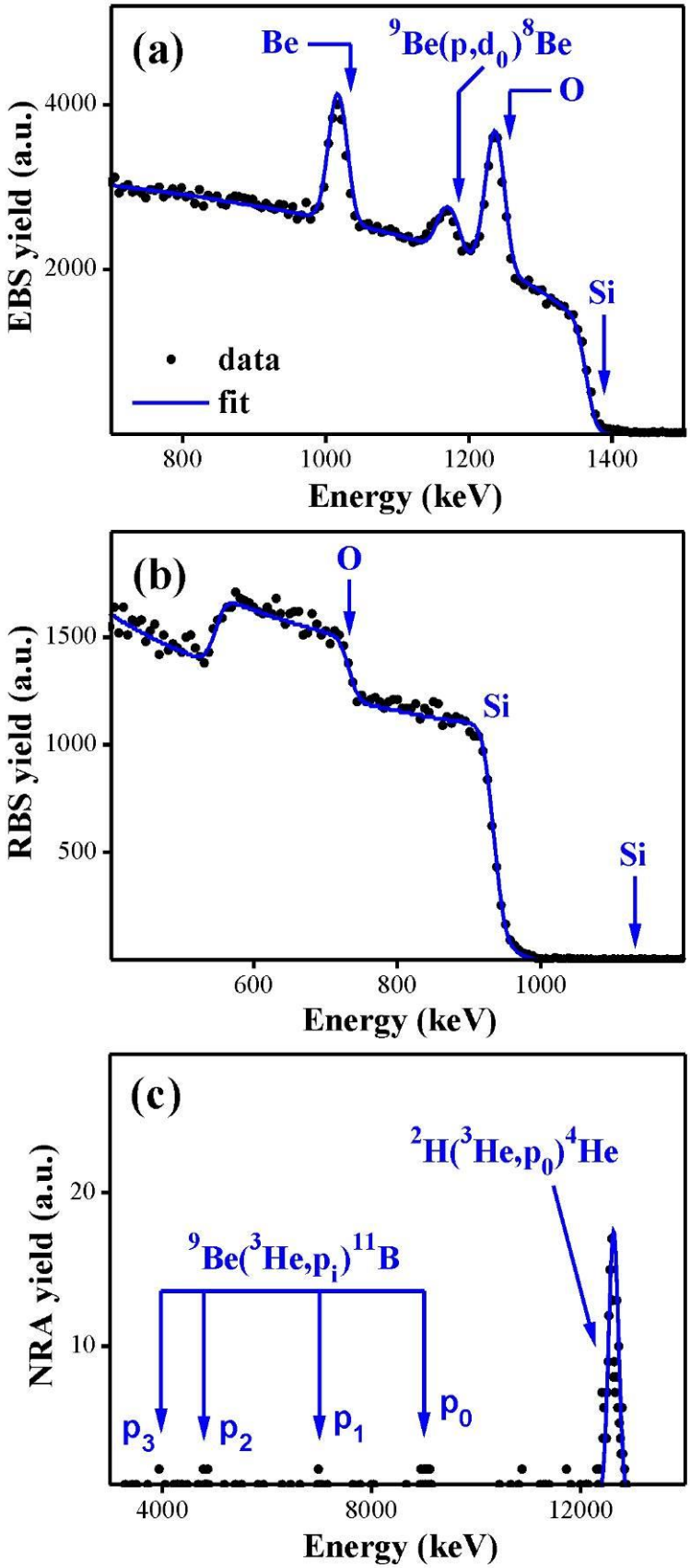
(a)
Be
^{9}Be(p,d$_0$)^{8}Be
O
Si
data
fit
EBS yield (a.u.)
4000
2000
800
1000
1200
1400
Energy (keV)
(b)
O
Si
Si
RBS yield (a.u.)
1500
1000
500
600
800
1000
Energy (keV)
(c)
^{2}H(^{3}He,p$_0$)^{4}He
^{9}Be(^{3}He,p$_i$)^{11}B
p$_3$
p$_2$
p$_1$
p$_0$
NRA yield (a.u.)
20
10
4000
8000
12000
Energy (keV)

Fig. 2

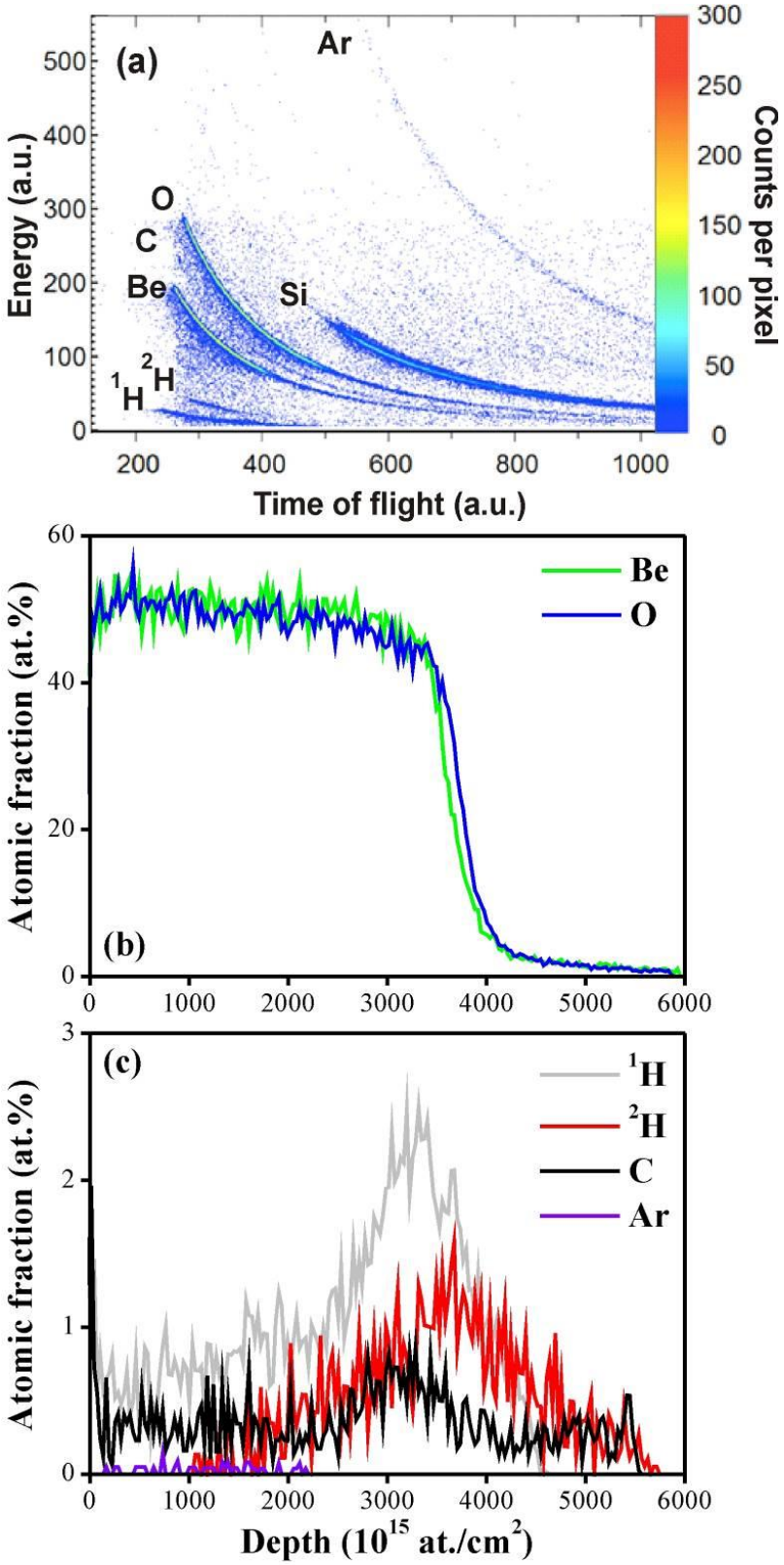
(a)
Ar
O
C
Be
Si
^{1}H
^{2}H
Energy (a.u.)
Time of flight (a.u.)
Counts per pixel
(b)
Be
O
Atomic fraction (at.%)
(c)
^{1}H
^{2}H
C
Ar
Atomic fraction (at.%)
Depth (10^{15} at./cm^2)

Fig. 3